Channel and Energy Modeling for Self-Contained Wireless Sensor Networks in Oil Reservoirs

Hongzhi Guo, *Student Member, IEEE,* Zhi Sun, *Member, IEEE*

***Abstract*—The real-time and in-situ monitoring capability in oil reservoirs is highly desired to increase the current recovery factor of crude oil and natural gas. To this end, the wireless sensor networks (WSNs) are envisioned to be deployed deep inside oil reservoirs to collect and report the physical and chemical information in real time. However, none of the existing wireless communication and networking technologies can support WSNs in oil reservoirs due to the very challenging environment and the extremely small device size. To address the problem, this paper proposes a new self-contained micro wireless sensor network framework based on the Magnetic Induction (MI) technique, which can enable the real-time and in-situ monitoring in oil reservoirs. Rigorous analytical models are developed to characterize the oil reservoir channel for both MI communication and energy transfer, which confirm the feasibility of the proposed self-contained sensor network framework. To enhance the system efficiency and reliability, high-permeability proppants are injected in the hydraulic fracture to increase mutual induction; while the tri-directional MI coil antenna is designed to achieve omnidirectional coverage. The theoretical models and numerical results are validated by the widely used finite element simulation software COMSOL Multiphysics.**

***Index Terms*—Channel modeling, oil reservoirs, Magnetic Induction (MI) communications, wireless sensor networks, self contained, wireless energy transfer.**

I. Introduction

CURRENTLY the crude oil and natural gas provide more than 50% share of the total global energy consumption. However, the oil reserve is diminishing faster and faster due to the increasing energy demands all over the world. Meanwhile, the current achievable oil recovery rate, i.e. the ratio of recoverable oil to the total oil in the reservoirs, is less than 60% even using the latest extraction technologies [2], which aggravates the global energy crisis. Hence, to guarantee the global energy security, it is of great importance to increase the current oil recovery factor.

Increasing recovery factor requires optimally developing the oil/gas fields and optimally managing the recovery process, which necessitates the real-time and high resolution physical/chemical information throughout the whole oil reservoirs, such as pressure, temperature, and fluid type. Better understanding of such information in oil reservoirs can significantly increase the recovery factor. For instance, during the recovery process, water is injected into the oil reservoir to maintain the pressure. On the one hand, if the injected pressure is too low, the oil cannot be effectively extracted. On the other hand, if the pressure is too high, the reservoir can be destroyed. Hence, by deriving the real-time pressure information inside oil reservoirs, the water injection can be optimally managed and the oil recovery factor is envisioned to be increased by 15%-25% [3].

However, to date, no existing technology can provide the real-time and in-situ monitoring capability *inside* oil reservoirs [4], [5]. The accuracy of remote monitoring [6], [7] are far from satisfactory, while the intra-wellbore monitoring systems [8] cannot derive the measurements deep inside the oil reservoirs.

A natural idea to collect the accurate real-time information is to utilize the wireless sensor network (WSN) paradigm [9], where wireless sensors are deployed throughout the whole oil reservoir. Such kind of in-situ and direct measuring techniques have drawn increasing attention from the industry and research community. Currently, most of the efforts have been put towards the development of the sensors that are small and strong enough for the deep oil reservoir monitoring [2]. This kind of micro wireless sensor motes have been successfully injected into oil reservoirs [10].

However, it is still unknown how to continuously report the measurements from the micro wireless sensors deep inside oil reservoirs in real time. Existing wireless communication and networking solutions do not support WSNs in the oil reservoirs. Specifically, Fig. 1 shows the typical oil reservoir environment and the oil extraction process, where a wellbore is drilled to the underground oil reservoirs at the depth of around 6,000 ft. The hydraulic fracturing process using high pressure fluid to open several long but very narrow fractures growing from the wellbore to the targeted rock formations, so that the oil and natural gas can be extracted. The length of the fracture can reach up to 100 m; while the typical width and height of the fracture are 0.01 m and 1 m, respectively. Since the WSN is envisioned to be deployed in the fractures during the hydraulic fracturing process, the following research challenges are imposed to the existing wireless communication and networking solutions:

- *Extremely high path loss in oil reservoirs*: Since the oil reservoirs consist of crude oil, gas, soil and rocks, and other injected fluids, electromagnetic (EM) waves experience significant material absorptions. Consequently, the path loss in the oil reservoir is extremely high.
- *Infeasibility in radiating wireless signals*: Due to the very narrow fracture, the size of wireless sensors should be no larger than 1 cm. Consequently, the antenna on the sensor node can only radiate EM waves with a frequency of

Manuscript received May 8, 2013; revised September 6, 2013 and November 20, 2013; accepted January 23, 2014. The associate editor coordinating the review of this paper and approving it for publication was M. Vu.

A much shorter preliminary version of this paper appeared in [1]

The authors are with the Department of Electrical Engineering, University at Buffalo, the State University of New York, Buffalo, NY 14260, United States (e-mail: {hongzhig, zhisun}@buffalo.edu).

Digital Object Identifier 10.1109/TWC.2013.130835

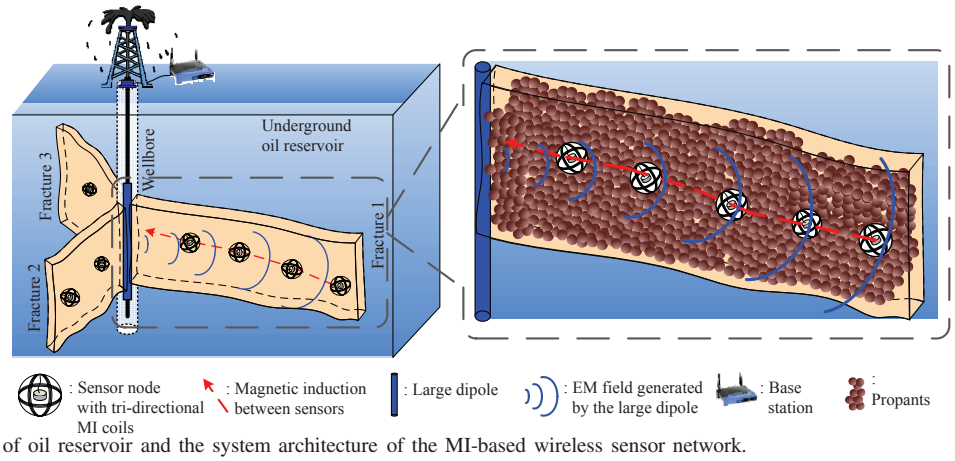

Fig. 1. The structure of oil reservoir and the system architecture of the MI-based wireless sensor network.

hundreds of GHz or even several THz. The propagation of such high frequency signals in the oil reservoirs is extremely difficult [11].

- *Prohibitively short system lifetime*: Similarly, due to the size limitation, the capacity of the battery on the wireless sensor is extremely small. The small battery cannot power the device for a long enough operating period, which causes a prohibitively short system lifetime of the wireless sensor networks in oil reservoirs.

To address the above research challenges, in this paper, we propose a new self-contained micro wireless sensor network framework based on the Magnetic Induction (MI) technique [12], which enables the in-situ, real-time, and long system-lifetime monitoring in the harsh oil reservoir environments. Specifically, instead of using EM waves and the dipole antenna, the micro sensor nodes use MI coil antenna to generate and receive the wireless signals through the magnetic coupling. The near field of the magnetic field generated by the micro MI coil can penetrate the high loss oil reservoir channel more efficiently, which is utilized to realize the wireless communication. Moreover, the MI technique can be utilized for wireless energy transfer [13]. Here, We use the dipole antenna to wirelessly power the micro sensor nodes deep inside oil reservoirs.

It should be noted that, wireless communication in challenging environments, especially in underwater, have been extensively explored. However, the results cannot be applied to the oil reservoir environment due to the following reasons. Firstly, the highly confined space can significantly affect the field distribution, which leads to very complicated channel characteristics in oil reservoir. Moreover, most underwater communication system utilizes acoustic waves, which is different from the magnetic induction. Secondly, we can artificially modify the electromagnetic properties of the signal propagation medium in the oil reservoirs. Thirdly, the power issue is much more critical for the sensors in oil reservoir. For the sensors in oil reservoir, once they are injected into the fracture, there is no way to replace them. Thus we need to design self-contained sensor network.

Generally, our contributions in this paper are summarized as follows:

1) We for the first time propose a self-contained wireless sensor network framework that can work in the extremely small and harsh fracture environments deep inside oil reservoirs. To date, this is the only possible solution to realize the real-time and in-situ monitoring in oil reservoirs. Through theoretical modeling and simulation validation, we show the proposed real-time monitoring capability can reach at least 40 m inside the fractures in oil reservoirs while the interval between the millimeter-scale sensor nodes can be as large as 1 m.
2) We develop rigorous analytical models to characterize the signal and energy propagations in the hydraulic fractures in oil reservoirs, which lays the theoretical foundation for both the MI communication and the wireless energy transfer in the proposed self-contained wireless sensor network framework.
3) Based on the channel models, we design two enhancement strategies to further improve the efficiency and reliability of the proposed oil reservoir sensor network, including 1). injecting high-permeability proppants in the hydraulic fracture to increase mutual induction; and 2). employing the tri-directional MI coil antenna to achieve omnidirectional coverage.

The remainder of this paper is organized as follows. The proposed oil reservoir wireless sensor network framework is introduced in Section II. Next, in Section III, the analytical channel models in the fracture environments in oil reservoirs are developed. The simulation and numerical results are also discussed to validate the theoretical model and to guide optimal system designs. After that, in Section IV, the energy consumption and transfer model of the whole sensor network system is developed based on the derived channel models. Then the optimal system parameters are determined and the self-contained property of the proposed framework is proved. Finally, this paper is concluded in Section V.

II. System Architecture and Operational Framework

The two-layer system architecture of the MI-based sensor network is illustrated in Fig. 1:

- The micro wireless sensors in the oil reservoir fracture form the first layer. They are injected into the fracture during the hydraulic fracturing process. The sensor nodes equipped with tri-directional coil antenna are tethered by a thin thread to control their positions. As a result, the positions of the sensors are approximately uniform and linear inside the fracture. However, the orientation

of the coils cannot be controlled. At the end of the hydraulic fracturing process, proppants are injected to prevent the fracture from collapsing [4], which can also fix the positions of the sensors inside the fracture. The wireless sensor nodes have no power source but can be wirelessly charged by the radiation of the large dipole antenna inside the wellbore. What's more, the MI sensor nodes are wirelessly connected to each other by the MI communication mechanism.

- The base station forms the second layer. It consists of a large dipole antenna at the wellbore and an aboveground gateway. Since dipole antenna has high transmission power, it can use MHz frequency EM wave signals and effectively transfer both the information and energy through the oil reservoir medium to the micro MI sensor nodes inside the fracture.

Noted that, the thread tethering the sensors can also be used for energy transfer and communications. However, in the harsh oil reservoir environments, the thin threads are prone to fail. If the system only depends on the threads to get power and communicate, a break at any point along the thread can cause the whole system fail. Therefore, although the final product of the oil reservoir sensor network can be a hybrid wired and wireless system, this paper focuses on the wireless techniques, since many existing techniques can realize the wired energy transfer and communications but the research on wireless systems in oil reservoir is still a void so far.

Based on the system architecture, a three-phase operational framework is proposed as follows:

- In the first phase, the base station uses the large dipole antenna to radiate energy into the fracture and activate the micro wireless sensors using the inductive charging technique. Then the base station sends a data request to one or a group of selected sensor nodes using the MI communication mechanism, which forms the one-hop downlink channel. In the next section, we propose to add high permeability (high-μ) additive to the proppants, which can greatly enhance the magnetic coupling so that the performance of wireless communications and energy transfer in the oil reservoir fractures can be improved.
- In the second phase, the passive wireless sensors in the fracture are activated by the magnetic field radiated by the large dipole antenna of the base station. After the sensors obtaining enough energy, they start to measure the physical reservoir properties such as pressure, temperature, oil saturation, fluid type, among others. Then the sensors send the sensing results back to the base station, which forms the uplink channel. Since the size of the sensor node is very small and has no power source, it is impossible to send the measurements back to the base station in one hop. Therefore, the micro sensor nodes utilize the MI communication mechanism to transmit the measurements to the nearest neighbor node. By the consecutive relaying, the uplink with a multi-hop transmission route is formed to transmit the data back to the base station. Moreover, to enhance the system reliability, we employed the tri-directional coil antenna on each sensor to achieve omnidirectional coverage.

(a) Downlink (b) Uplink

Fig. 2. Channel between TX and Unidirectional RX

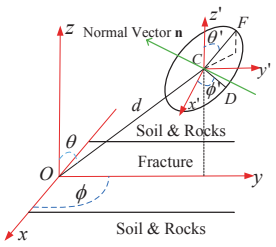

Fig. 3. Coordination of the system.

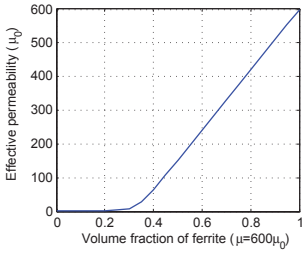

Fig. 4. Effective permeability of proppants.

- In the third phase, the base station receives the sensing results from all the selected sensors in the fractures. Then the base station forwards the data through the aboveground gateway to the remote administration center via terrestrial wireless communication techniques, such as satellite and cellular networks.

III. Channel Modeling in Oil Reservoirs

The major objective of this paper is to prove the feasibility and the effectiveness of the oil reservoir wireless sensor network framework proposed in Section II. To this end, we investigate 1). the wireless channel in oil reservoirs for both MI communications and energy transfer in this section, and 2). the energy consumption and transfer model of the entire sensor network system in the next section.

The proposed oil reservoir sensor network system consists of two types of channels: 1) the down link channel from the large dipole on the base station to the micro MI coils on the sensor nodes, which is used to transfer energy and transmit data request from the base station to the sensor nodes, as shown in Fig. 2(a); and 2) the uplink channel between MI coils on two adjacent sensors, which is used to send and relay the measurement data from the sensor nodes to the base station in the multi-hop fashion, as shown in Fig. 2(b). It should be noted that the channel analysis on the last hop in the uplink, i.e. the channel from the last coil to the dipole antenna, is neglected. Since once the data is relayed to a coil which is close to the dipole antenna, it is easy to accomplish the last step and the analysis is trivial. Hence, in the rest part of this section, we concentrate on the two important channels: the channel between dipole and coil, and the channel between two coils. First, we develop the analytical models for the two important channels in the high-μ fracture environment, which shows that the high-μ proppants can indeed help the wireless communications. Then, the theoretical models are validated by the Comsol Multiphysics-based simulations. The unique oil reservoir channel characteristics are also discussed

based on the numerical and simulation results. Finally, the tri-directional coil antenna is proposed and analyzed to enhance the reliability of the proposed MI communications and energy transfer in oil reservoirs.

A. Modeling Downlink Channel

No matter in the downlink channel or in the uplink channel, the orientation of the coil antenna on each sensor node is highly random. Hence, it is important to model the effects of the coil with random orientations. In the rest sections of this paper, we use a normal vector $\mathbf{n}$ to denote the orientation of the coil. The way to analytically derive the normal vector is explained in the Appendix. As shown in Fig. 3, the coordination of the system is set as follows. The origin is the midpoint of the dipole antenna. The width of the fracture is x axis, the length of the fracture is y axis, and the height of the fracture is z axis. The center of the coil is denoted by (d, θ, ϕ). The orientation of the coil is expressed by two angles (θ', ϕ'). θ and θ' are the polar angles and ϕ and ϕ' are the azimuthal angles, as shown in Fig. 3. For example, when the axis of the coil is parallel with y axis, the orientation of such coil is determined by $\theta' = 0$ and $\phi' = 0$.

In the downlink channel, the large dipole antenna generates an EM field in MHz frequency range and utilizes this field to transfer energy and transmit data signal to the micro sensor nodes in the fracture. In this subsection, we first analyze the distribution of the magnetic field in the fracture. Then based on the magnetic field distribution, the channel path loss is derived.

1) Effective permeability in oil reservoir: Before deriving the channel model, we briefly introduce the way to increase the effective permeability in oil reservoirs. Firstly, we add high-μ material, i.e. ferrite, into the proppant to increase its effective permeability. Then, the high-μ proppants are injected into the fracture during the hydraulic process to create the high-μ environment.

According to the Effective Medium Theory [14], the effective parameter of a mixture can be expressed as

$$\sum_{i=1}^{N} f_i \frac{\mu_i - \mu_{eff}}{\mu_i + 2\mu_{eff}} = 0, \tag{1}$$

where μ_{eff} is the effective permeability, N is the number of the materials in the mixture. The volume fraction of the i^{th} material f_i is subjected to $\sum_{i=1}^{N} f_i = 1$. As shown in the equation, the effective permeability is determined by the permeability of each additive and its volume fraction. Ferrites are non-conductive ferrimagnetic ceramic compounds. The permeability of the ferrites can be higher than 600 μ_0. Currently, ceramic proppants are widely used in the oil industry. Thus, we can manipulate the volume fraction of the ferrites in proppants to get the expected effective permeability. If we assume the original permeability of the proppants is μ_0, and we add ferrites with permeability 600 μ_0 into the proppants, the relation between the volume fraction of the additive and the effective permeability of the proppants is shown in Fig. 4. As presented in the figure, even the volume fraction of the ferrites is less than half, we can easily get more than 100 μ_0.

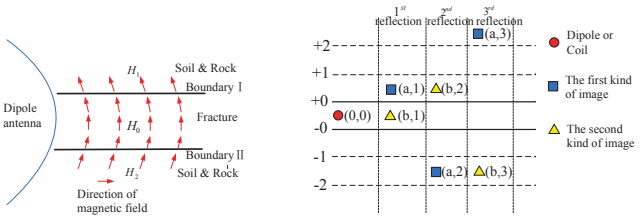

(a) Direction of magnetic field in the fracture.

(b) Images of the source in the fracture (top view).

Fig. 5. Illustration of the magnetic field direction and image method.

Then proppants are injected into the fractures. The transmission medium in the fracture is filled with crude oil, gas, injected fluids, among others. Since these components have different dielectric properties, the environment is inhomogeneous for the EM field. To address this problem, we utilize the EMT again to find the effective dielectric parameters of the fracture medium. The prerequisite to use this theory here is that the wavelength should be much larger than the size of the component. Since the operating frequency of the proposed system is around 10 MHz and the size of the components of the fracture medium in the oil reservoir is much smaller than 0.01 cm, the EMT can be well applied in the oil reservoir environments. Then, the environment can be modeled as homogeneous for the EM field. Since the proppants accounts for more than half of the space in the fracure, and their permeability can be adjusted by changing the volume fraction of the ferrites, we can get the desired effective permeability in the fracture.

2) Magnetic field distribution in downlink: Due to the high-μ additive and the complicated environment, the dielectric properties inside and outside the fracture are dramatically different. Thus, the EM field experiences significant reflections. In this paper, the image theory [15] is used to analyze the reflections. We assume the effective permeability, permittivity and conductivity inside the fracture are μ_1, ϵ_1, and σ_1, respectively, while the soil and rocks outside the fracture have the effective permeability μ_2, permittivity ϵ_2, and conductivity σ_2. The length, input current, and input resistance of the dipole antenna are l, I_0, and R_i, respectively. The radius, resistance, and number of turns of the coil are r, R_c, and N, respectively. According to the antenna theory [16] and the analysis of conductive medium loss [17], the magnetic field around the antenna is given by:

$$\mathbf{H} = \mathbf{a}_\phi \cdot \frac{kI_0 l \sin\theta}{4\pi d} \cdot \left[\frac{1}{kd} + j\right] \cdot e^{-jkd - d/\delta}, \tag{2}$$

where d is the distance; k is the wavenumber; δ is the skin depth, which is given by $\delta = 1/(\omega\sqrt{\mu\epsilon/2(\sqrt{1+\sigma^2/(\omega^2\epsilon^2)}-1)})$, where ω is the angular frequency.

To apply the image theory to characterize the reflections, the boundary conditions between the inside and outside of the fracture need to be investigated. Since the sensor nodes are injected in the middle of the fracture, the top and the bottom boundaries are too far away from the sensor nodes compared with the left and the right boundaries. Therefore, we only consider the left and the right boundaries. Moreover, as shown in Fig. 5(a), the magnetic field generated by the electrical

antenna only has $\mathbf{H}_\phi$ and the direction of the magnetic field surrounds the dipole antenna is a circle. In Fig. 5(a), the magnetic field first penetrates the Boundary II. Then it is reflected by Boundary I. Thus, for Boundary I, the magnetic field is from inside to outside and for Boundary II, the direction is reversed. As a result, they have different boundary conditions that need separate analysis.

a) Boundary conditions I: As shown in Fig. 5(b), we assume the source is located at the middle of the fracture. For the boundary +0 (which is Boundary I in Fig. 5(a)), the original source has two images: one is $(a, 1)$ on the other side of the boundary +0 and the other one is at the same position as the original source. Since only the source and the image $(a, 1)$ determine the magnetic field in the fracture, we only show them in Fig. 5(b). In addition, due to the existence of the boundary -0 (which is Boundary II in Fig. 5(a)), the image $(a, 1)$ acts as a new source and create a new image $(a, 2)$. So on and so forth, infinity number of images are created. It should be noted that reflection can change the direction of the magnetic field. As a result, the magnetic fields generated by images have opposite direction to their sources.

Now, we have $\mathbf{H}_0$ and $\mathbf{H}_R$ inside the fracture and $\mathbf{H}_1$ and $\mathbf{H}_T$ outside the fracture. $\mathbf{H}_0$ and $\mathbf{H}_1$ are the magnetic fields generated by the dipole antenna without any reflection and transmission. $\mathbf{H}_R$ and $\mathbf{H}_T$ are the magnetic fields created by the reflection and transmission on Boundary I. The fields at the two sides of the boundary follows the relationship defined by Maxwell equations. We utilize the property that the tangential component of the magnetic field $\mathbf{H}$ is continuous and the normal component of the magnetic flux density $\mathbf{B}$ is continuous. Therefore,

$$\begin{cases} (\mathbf{H}_0 + \mathbf{H}_R) \cdot \mathbf{t} = (\mathbf{H}_1 + \mathbf{H}_T) \cdot \mathbf{t} \\ \mu_1 (\mathbf{H}_0 + \mathbf{H}_R) \cdot \mathbf{n} = \mu_2 (\mathbf{H}_1 + \mathbf{H}_T) \cdot \mathbf{n} \end{cases} . \tag{3}$$

where $\mathbf{t}$ is the tangential vector, and $\mathbf{n}$ is normal vector. According to the definition of the image, all the magnetic fields of the images have the same form. The differences are the dielectric properties of the medium, the input current and the distance. By substituting (2) into (3), we can find the input current of $\mathbf{H}_R$, which is:

$$I_R = \frac{\mu_1 - \mu_2}{\mu_1 + \mu_2} I_0 . \tag{4}$$

For the n^{th} reflection, the input current of the image is:

$$I_{Rn} = \left(\frac{\mu_1 - \mu_2}{\mu_1 + \mu_2}\right)^n I_0 . \tag{5}$$

b) Boundary conditions II: For Boundary II, since the direction of the magnetic field is from outside to inside, we need to consider the transmitted portion of the magnetic field. According to the image theory, one image is located at the same position as the source and the other one is outside the fracture. In this case only the image at the same position as the source can influence the magnetic field distribution in the fracture and it is denoted by the triangular $(b, 1)$ in Fig. 5(b). Similarly, image $(b, 1)$ can act as a source and create a new image $(b, 2)$, which means the transmitted magnetic field from outside of the fracture is reflected by the boundary +0. Then, the situation is the same as the analysis of Boundary Condition I. Similarly, we can obtain the input current of image $(b, 1)$, which is:

$$I_T \simeq \left(\frac{2\mu_2 k_2}{(\mu_1 + \mu_2) k_1} e^{d/\delta_1 - d/\delta_2} - 1\right) I_0 . \tag{6}$$

The input current of the n^{th} image caused by reflections is

$$I_{Tn} \simeq \left(\frac{2\mu_2 k_2}{(\mu_1 + \mu_2) k_1} e^{d/\delta_1 - d/\delta_2} - 1\right) \left(\frac{\mu_1 - \mu_2}{\mu_1 + \mu_2}\right)^{n-1} I_0 \tag{7}$$

c) Magnetic field in the fracture: The magnetic field at any point inside the fracture is the superposition of the magnetic fields of the original dipole antenna and all the images. The position of each image is defined by Fig. 5(b) and the input current of each image is given by (5) and (7). So the magnetic field is:

$$\begin{aligned} \mathbf{H} \simeq & \sum_{n=0}^{\infty} \mathbf{a}_{\phi n} \frac{I_0 l \sin\theta_n}{2\pi d_n} \frac{\mu_2 k_2}{(\mu_1 + \mu_2)} \\ & \cdot \left(\frac{\mu_1 - \mu_2}{\mu_1 + \mu_2}\right)^n \left[\frac{1}{k_1 d_n} + j\right] e^{-d_n/\delta_2 - j k_1 d_n} . \end{aligned} \tag{8}$$

3) Path loss for downlink channel: The received power at a sensor node is determined by two factors: the magnetic filed derived from (8), and the orientation of the MI coil on the sensor, which is expressed as the normal vector $\mathbf{n}$ of the coil that is derived in the Appendix. After deriving these two factors, the electromotive force at the receiving coil can be calculated by:

$$emf = N \frac{d\mathbf{B}}{dt} \cdot \mathbf{S}_{coil} \simeq N \mu_1 \pi r^2 \frac{d}{dt} \mathbf{H} \cdot \mathbf{n} . \tag{9}$$

Then, the maximum received power with matched load at the receiving coil is calculated by:

$$P_{RX,d2c} = \frac{1}{2} \left(\frac{|emf|}{2R_c}\right)^2 \cdot R_c = \frac{|emf|^2}{8R_c} . \tag{10}$$

After that, by substituting (8) in (9), the received power in (10) can be obtained.

Meanwhile, the transmission power at the dipole antenna is:

$$P_{TX,d2c} = \frac{1}{2} I_0^2 R_i . \tag{11}$$

Then, the path loss of the downlink channel can be calculated based on (10) and (11):

$$\begin{aligned} L_p^{d2c} \simeq & -10lg\left(\frac{P_{RX,d2c}}{P_{TX,d2c}}\right) \simeq -10lg \left\{ \frac{N^2 \omega^2 r^4 l^2 \mu_1^2 \mu_2^2 k_2^2}{16 R_c R_i (\mu_1 + \mu_2)^2} \right. \\ & \left. \left| \sum_{n=0}^{\infty} \frac{\sin\theta_n}{d_n} \left(\frac{\mu_1 - \mu_2}{\mu_1 + \mu_2}\right)^n \left[\frac{1}{k_1 d_n} + j\right] e^{-d_n/\delta_2} \mathbf{a}_{\phi n} \cdot \mathbf{n} \right|^2 \right\} . \end{aligned} \tag{12}$$

Due to the narrow fracture, all the images are close to each other. Moreover, the magnetic field strength of high order images becomes very weak after many times of reflections. Therefore, we can assume that all the images are at the same position and have the same magnetic field direction as the source. However, the sign of the magnetic field strength should be different between the image and its source, i.e. if the source

is positive, the image should be negative. As a result, the path loss for downlink channel (12) can be simplified as:

$$L_p^{d2c} \simeq -10lg\left\{\frac{N^2\omega^2\mu_2^2 l^2 r^4 k_2^2 \sin^2\theta}{64R_cR_id^2}\left[\frac{1}{k_1^2d^2}+1\right]e^{-2d/\delta_2}\right\}. \tag{13}$$

B. Modeling Uplink Channel

In the uplink channel, the sensor nodes utilize the MI communication mechanism to send the measurement data back to the base station. A multi-hop route is formed from the transmitter sensor nodes to the dipole antenna through the intermediate relay sensor nodes. In this subsection, the magnetic field generated by a coil is first investigated. Then, the path loss of the uplink channel is calculated.

1) Magnetic field distribution in uplink: The small coil can be modeled as a magnetic dipole. Hence, the magnetic field around it can be calculated by [15]:

$$\mathbf{H}_0 \simeq \frac{NI_0r^2}{4}\left(\mathbf{a}_r\frac{2}{d^3}\cos\theta+\mathbf{a}_\theta\frac{1}{d^3}\sin\theta\right)e^{-j\omega t-d/\delta}. \tag{14}$$

In this paper, we only consider the near filed of a coil since the envisioned communication range here is much smaller than the wavelength of the signal. Similar to the analysis on downlink channel, we use the image method and setup the images for the source, as shown in Fig. 5(b). The image settings are exactly the same as in the downlink case. However, for the boundary conditions, there is no other magnetic fields outside the fracture, except for the transmitted field of the magnetic dipole, i.e. there is no H_1 and H_2 outside the fracture since the dipole antenna is not working when the sensor nodes are communicating with each other. In this case, the two boundaries have the same situation. Therefore, the input current of the n^{th} coil image is given by:

$$I_{Rn} \simeq \left(\frac{\mu_1-\mu_2}{\mu_1+\mu_2}\right)^n I_0. \tag{15}$$

For each reflection, there are two images located outside the fracture. Here we use $\mathbf{H}_{ni}$ to denote the magnetic filed generated by the image, where n is the n^{th} reflection and i is the image generated by the i^{th} boundary. Then, the magnetic field in the fracture is:

$$\mathbf{H} = \mathbf{H}_0 + \sum_{n=1}^{\infty}\sum_{i=1}^{2}\mathbf{H}_{ni}. \tag{16}$$

Different from the dipole antenna, the transmitting coil can have arbitrary orientation, as discussed previously. This arbitrary orientation is identified by the normal vector $\mathbf{n}$ given in the Appendix. Since we know the center of the coil, then for any point in the fracture, we can find an unit vector whose direction is from the center of the coil to the point and it is denoted by $\mathbf{a}_r$. By utilizing $\mathbf{a}_r$ and the normal vector $\mathbf{n}$ of the coil, we can obtain θ and $\mathbf{a}_\theta$. Then, the magnetic field in uplink given in (16) can be further developed as:

$$\mathbf{H} \simeq \frac{NI_0r^2}{4}\left[\left(\mathbf{a}_{r_0}\frac{2\cos\theta_0}{d_0^3}+\mathbf{a}_{\theta_0}\frac{\sin\theta_0}{d_0^3}\right)e^{-j\omega t_0-d_0/\delta_1} + \sum_{n=1}^{\infty}\sum_{i=1}^{2}\left(\frac{u_1-u_2}{u_1+u_2}\right)^n\left(\mathbf{a}_{r_{ni}}\frac{2\cos\theta_{ni}}{d_{ni}^3}+\mathbf{a}_{\theta_{ni}}\frac{\sin\theta_{ni}}{d_{ni}^3}\right)e^{-j\omega t_{ni}-d_{ni}/\delta_1}\right]. \tag{17}$$

2) Path loss for uplink channel: The mutual induction between two unidirectional coils can be approximately expressed as:

$$M \simeq \frac{N\Phi}{I_0} \simeq \frac{N\mu_1\pi r^2|\mathbf{H}\cdot\mathbf{n}|}{I_0}, \tag{18}$$

where $\mathbf{n}$ is the normal vector of the receiving coil given in the Appendix. The path loss of the MI communication between the two MI transceivers can be expressed as:

$$L_p^{c2c} \simeq -10lg\left[\frac{\omega^2M^2}{2R_c\left(R_c+\frac{\omega^2M^2}{R_c}\right)}\right]. \tag{19}$$

Then by substituting (18) into (19), the path loss of the uplink channel between two MI coils in the oil reservoir is derived.

C. Simulation Validation and Channel Characteristics in Oil Reservoirs

So far, the theoretical models for downlink channel and uplink channel have been developed in the previous two subsections. In this subsection, we first utilize the Comsol Multiphysics to simulate the magnetic field distribution in the fracture to validate the theoretical models. Then, the channel characteristics in oil reservoirs are discussed based on the theoretical and simulation results. The default parameters are set as follows. The permeability of the soil and rock is similar to that of air, i.e. $\mu_2 = \mu_0 = 4\pi\times10^{-7}$ H/m. The effective permeability inside the fracture is $\mu_1 = 20\mu_0$ due to the injected high-μ proppants. This effective permeability can be controlled by the material used to produce the high-μ proppants, according to the EMT [14]. In Section IV, we discuss the way to find the optimal μ_1.

The permittivity of the soil and rock is set to be $\epsilon_2 = 2\epsilon_0$ (sand and clay mixture) while the effective permittivity inside the fracture is set to be $\epsilon_1 = 3.5\epsilon_0$ (crude oil), where ϵ_0 is the permittivity of the air. Since the injected water accounts for a very small portion in the fracture, according to the EMT, the effective conductivity is very low. We set the conductivity inside the fracture is $\sigma_1 = 10^{-4}$ S/m, while the conductivity outside the fracture is set to be $\sigma_2 = 0.001$ S/m. A 20 m long base station dipole antenna is used with the transmission power of 5 KW. The input resistance is $R_i = 75\Omega$. The operating frequency is 10 MHz for both the dipole antenna and the coils. The coils have the radius of 5 mm and the number of turns is 10. The coil resistance is $R_c = 0.2\ \Omega$.

The simulation model in Comsol Multiphysics for downlink channel is shown in Fig. 6(a). In this model we set the length of the fracture is 20 m and use Perfectly Matched Layer (PML) in order to limit the modeling domain to save time and computational resources. PML can absorb all the propagating waves and mimic the real unbounded environment. All the inner boundaries are set as default which is the real situation in reality. The width and height of the fracture are 0.01 m and 1 m respectively. The dielectric parameters are the same as previous discussions. Fig. 6(b) compares the simulation result with the theoretical result derived by (8), which shows a very good match. Based on the distribution of the magnetic field, the received power by a unidirectional coil that has ideal orientation (planarly placed along the fracture) is shown in

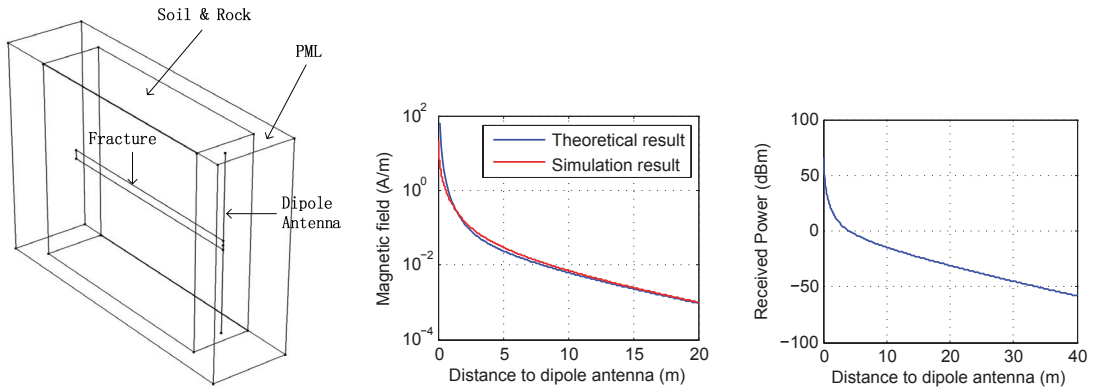

(a) Simulation model. (b) Magnetic field attenuation. (c) Received Power.

Fig. 6. Simulation of the downlink channel.

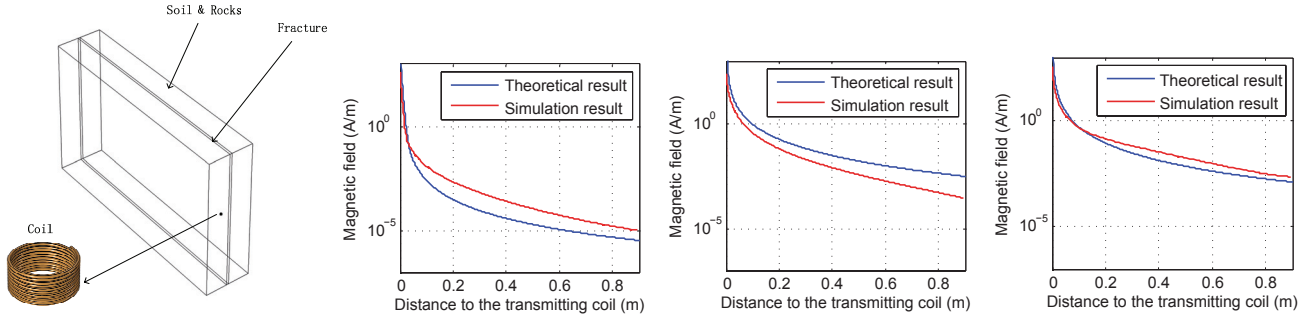

(a) Simulation model. (b) coil axis is x-direction. (c) coil axis is y-direction. (d) coil axis is z-direction.

Fig. 7. Simulation of the uplink channel.

Fig. 6(c). The received power at 40 m away from the dipole antenna can be around -60 dBm, which is possible to charge the ultra-low power wireless sensors operating at several micro watts.

The Comsol simulation model for uplink channel is shown in Fig. 7(a). The geometric and electromagnetic parameters are the same as before. The current in the coil is 1 A. The radius of the coil is 0.005 m and the size of the fracture is the same as the simulation for the downlink channel. Here we use relatively large geometry for soil and rocks outside the fracture to reduce the effect of reflection from the boundaries of the model. Since the orientation of the coil is random, we provide the magnetic fields generated by three different unidirectional coils: the axis of the coil is x-direction Fig. 7(b), the axis of the coil is y-direction Fig. 7(c), and the axis of the coil is z-direction Fig. 7(d). All other orientations can be the combinations of the above three orientations. As shown in Fig. 7, the theoretical results derived by (17) match the simulation results very well.

The path loss between two unidirectional coils (both of them are the z-direction coils) is shown in Fig. 8. Since the wireless sensor nodes operate at ultra-low power mode, the transmitted power is lower than -20 dBm. As a result, the communication range cannot be arbitrarily long to guarantee the receiver derive enough signal power to correctly receive the data. According to Fig. 8, a 1 m transmission distance can be achieved for two adjacent micro sensors in the uplink if we requires the path loss less than 50 dB (i.e. the received power is higher -80 dBm).

In the proposed MI-based wireless sensor network, both the uplink channel and downlink channel are based on magnetic induction. Intuitively, if we increase the permeability, the magnetic flux can be enhanced. Fig. 9 shows the effects of the permeability on the path loss in the fracture. The observing point is set at 5 m away from the dipole antenna (for the downlink) and 1 m away from the transmitting coil (for the uplink). In Fig. 9, the path loss of the uplink channel is in inversely proportional to the permeability μ_1. However, the path loss of the downlink channel is almost a constant. The reason behind this phenomenon is that the magnetic field of the odd-numbered images of the dipole antenna have almost opposite direction to the dipole antenna. Thus, if we increase μ_1, according to (5), the input current of the images will increase, the negative effect will be stronger. Consequently, the magnetic field should be smaller. For the magnetic flux, the negative effect can be mitigated by the increasing of the permeability μ_1. As a result, the magnetic flux generated by the dipole antenna is almost a constant and the path loss is also a constant for different μ_1. Moreover, in (13), it shows that the path loss is not affected by μ_1 when distance is relatively large, which is consistent with the numerical analysis. For the z-direction coil, since all the images can enhance the magnetic filed and μ_1 is increasing, the magnetic flux will increase. Therefore, the high-μ proppant has no effect on the channel between dipole antenna and coil, but it can significantly reduce the path loss of the communication channel between coil and coil. However, in Section IV, we find that μ_1 cannot be too high since it can also reduce the channel bandwidth. We show that the optimal μ_1 in our proposed system is around $20\mu_0$ in Section IV.

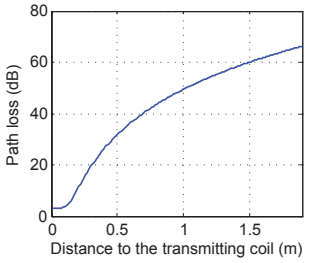

Fig. 8. Path loss between two unidirectional coils.

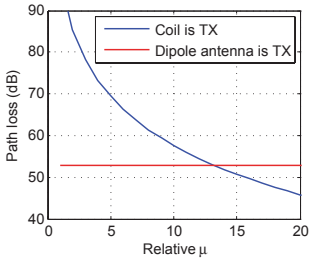

Fig. 9. The effect of high-μ.

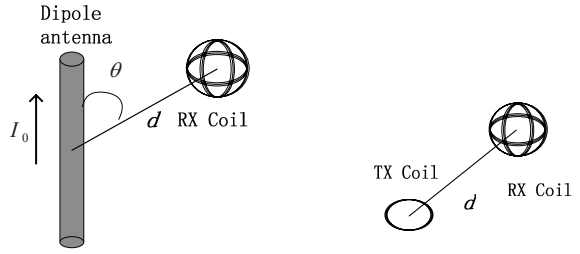

(a) Downlink (b) Uplink

Fig. 10. The downlink and uplink channel with tri-directional coil antenna.

D. Reliability Enhancement Using Tri-Directional Coil Antenna

According to the derived channel models, if the sensor node uses the unidirectional coil antenna, the system performance is very unreliable due to the uncontrollable coil orientations. To solve the problem, we propose to utilize the tri-directional coil antenna at the receiver, as shown in Fig. 10. The tri-directional coil antenna consists of three coils that are perpendicular to each other. This kind of coil antenna has been extensively used in both wireless communication and wireless power transmission [18], [19]. In particular, [20], [21], [22] use the tri-directional coil antenna to transmit power and information simultaneously. In this paper, we show that the sensor with tri-directional coil antenna is an omnidirectional receiver and the orientation almost has no effect on its performance.

1) Channel characteristics with tri-directional coil antenna: For the tri-directional coil, since the three unidirectional coils are orthogonal to each other, the received power can be calculated by:

$$P_{RX}^{tri} = P_{RX1} + P_{RX2} + P_{RX3}\ , \tag{20}$$

where P_{RXi} is the power received by the i^{th} unidirectional coil. When the transmitter is the dipole antenna, we can use the path loss of the downlink channel (13) to calculate P_{RX}^{tri}. Similarly, when the transmitter is the coil, we can use the path loss of uplink channel (19) to calculate P_{RX}^{tri}.

2) Performance evaluation: To prove the advantages of the tri-directional coil antenna, we numerically compare the performances of the systems using either unidirectional coil or tri-directional coil in both downlink and uplink channel. In the downlink, the distance between the dipole antenna and the sensor is set to be 10 m. The orientation of the dipole antenna is determined while the sensor node has arbitrary orientation. In the uplink, the distance between the transmitter sensor and the receiver sensor is set to be 1 m. As mentioned previously, even the tri-directional coil is utilized. the transmitter sensor only uses a single coil as the transmission antenna. Without loss of generality, we assume the transmitter sensor uses a coil that is the z-direction coil (for both the unidirectional coil system and the tri-directional coil system). We vary the orientations of the unidirectional coil and tri-directional coil by changing θ' and ϕ'. It should be noted that for tri-directional coil, its orientation is denoted by one of the unidirectional coils. Then the other two coils vary with the first one. Besides the above parameters, all the other system configurations are the same as previous sections.

When the receiver is the unidirectional coil, the path losses with different antenna orientations in downlink and uplink are shown in Fig. 11(a) and Fig. 12(a), respectively. In contrast, when the receiver is the tri-directional coil, the path losses with different antenna orientations in downlink and uplink are given in Fig. 11(b) and Fig. 12(b), respectively. If we assume the orientations of both tri-directional and unidirectional coils are uniformly distributed, the CDFs (cumulative distribution function) of the path loss distributions of the two types of coil antennas in downlink and uplink are given in Fig. 11(c), and Fig. 12(c), respectively. According to the results, the tri-directional coil antenna has much lower path loss and more reliable performance than the unidirectional coil when the antenna deviates from its optimal orientation.

IV. Energy Modeling and Self-Contained System Analysis

Based on the derived channel models, in this section, we show that the sensors deep inside oil reservoirs can utilize the energy transferred from the large dipole to perform sensing tasks and wirelessly transmit the measurements back to the base station. Specifically, the energy transfer model and energy consumption model for the proposed oil reservoir sensor network system are first developed. In order to calculate the transmitting/receiving time that is required by the energy consumption model, the uplink channel capacity is derived to obtain the achievable data rate. Then, based on the models, the self-contained property of the proposed wireless sensor network is validated by balancing the transferred energy and the consumed energy.

A. Energy Transfer Model

The downlink channel that is discussed in the last section is utilized here to realize the energy transfer. If the transmission power is P_{TX}^{dipole}, the received power at the MI sensor node is $P_{RX}^{coil} = P_{TX}^{dipole} \cdot L_p^{d2c}(d_{d2c})$, where $L_p^{d2c}(d_{d2c})$ is the path loss of the downlink channel given in (13) and the transmission distance is d_{d2c}. Assuming the energy conversion rate at the sensor node is η, the available power at the micro sensor node is:

$$P_{avail}^{sensor}(d_{d2c}) = P_{TX}^{dipole} \cdot L_p^{d2c}(d_{d2c}) \cdot \eta\ . \tag{21}$$

Then the energy transferred to the sensor node (denoted as node n) is $E_{rn} = P_{avail}^{sensor}(d_{d2c})T_c$, where T_c is the charging time. An ultracapacitor with capacity E_{max} is utilized by each sensor to store the energy. The sensors far away from the dipole antenna require more time to receive enough energy than those close to the dipole. However, since the sensor nodes that are far from the dipole do not need to relay as many packets as the sensor nodes near the dipole, they also requires less energy.

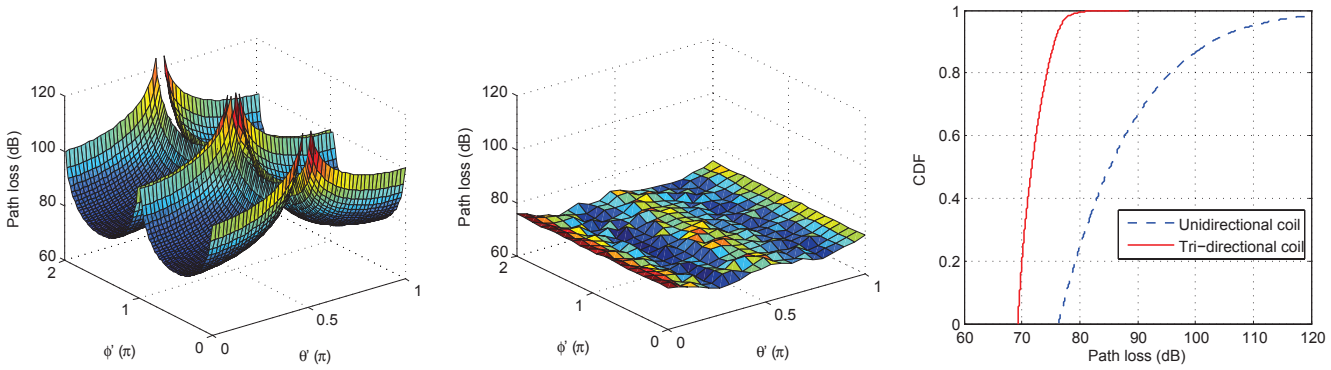

(a) Path loss of unidirectional receiver. (b) Path loss of tri-directional receiver. (c) CDF of path loss.

Fig. 11. Comparison between unidirectional coil and tri-directional coil in downlink channel.

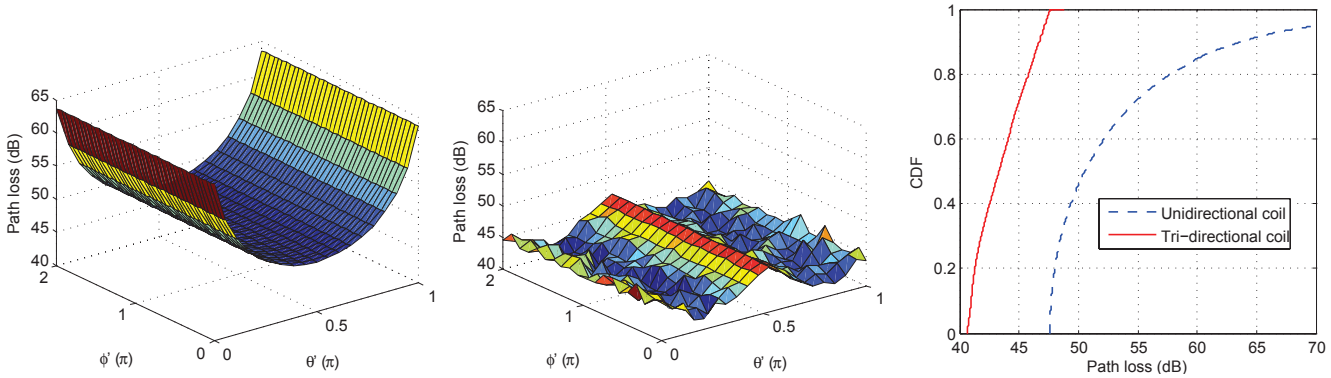

(a) Path loss of unidirectional receiver. (b) Path loss of tri-directional receiver. (c) CDF of path loss.

Fig. 12. Comparison between unidirectional coil and tri-directional coil in uplink channel.

B. Energy Consumption Model

We select a widely used energy consumption model given in [9], where the total energy consumption in a sensor node consists of three parts: the communication consumption, data processing consumption, and sensing consumption. Since the energy used for data processing and sensing constitutes a very small portion, only the communication energy consumption is considered in this paper.

The duty cycle of the proposed sensor network is denoted as T_0. During each cycle, all the sensor nodes report their measurements to the base station in turns. It costs E_t for sensor nodes to transmit the information and E_r for the relay nodes to receive the information. According to [23], $E_t = P_{tx}(T_{on-tx}+T_{st})+P_{out}T_{on-tx}$ and $E_r = P_{rx}(T_{on-rx}+T_{st})$. $P_{tx/rx}$ is the power consumption of the transmitter/receiver; P_{out} is the output transmit power; $T_{on-tx/rx}$ is the transmit/receive time; and T_{st} is the startup time of the transceiver. We assume the proposed sensor network has a linear topology along the long and narrow oil reservoir fracture. There are N sensor nodes in the network. We use sequence number n to denote each node. The sequence number of the sensor node who is the closest to the dipole antenna is 1. The next one is 2, so on and so forth. Then, the energy consumption in T_0 for each sensor node can be calculated by

$$E_{cn} = E_t + (N-n)(E_t + E_r); \tag{22}$$

Now the only unknown parameter in the energy model is $T_{on-tx/rx}$, i.e. the transmit/receive time, which is determined by 1). how much data needs to be transmitted/received and 2). how fast the data is transmitted/received. We assume the length of the measurement data that needs to be reported is a determined constant. Then, to complete the energy consumption model of the oil reservoir sensor networks, we only need to find out the data rate to report this data.

1) Uplink channel capacity: The upper bound of the data rate to report the sensing data is determined by the channel capacity of the uplink channel. It is shown in [24] that the MI energy transfer requires a single frequency to maximize the efficiency, while the MI communication needs a certain bandwidth. Thus, there should be an maximum value for the channel capacity. We have investigated the bandwidth and channel capacity of the MI-based wireless sensor networks with relay coils in [25]. In this paper, we further develop the result to cover the unique MI channel in the fracture environments in oil reservoirs. The 3-dB bandwidth in the oil reservoir sensor network can be obtained by:

$$\frac{\left|\frac{\omega^2M^2}{2(R_c+j\omega L+\frac{1}{j\omega C})^2+\omega^2M^2}\right|}{\frac{\omega^2M^2}{2R_c^2+\omega^2M^2}} = \frac{1}{2}, \tag{23}$$

where L and C are the coil inductance and the resonance capacitor. According to [25], $L \simeq \frac{1}{2}\mu_1\pi N^2 r$, while $C = \frac{1}{2\pi^3 f_0^2 N^2 \mu_1 r}$, where f_0 is the resonant frequency. By solving (23), we can obtain two frequencies: f_U that is the upper cutoff frequency; and f_L that is the lower cutoff frequency. Then the bandwidth of the uplink channel is:

$$B = f_U - f_L \simeq \frac{R_c}{\mu_1\pi^2N^2r}. \tag{24}$$

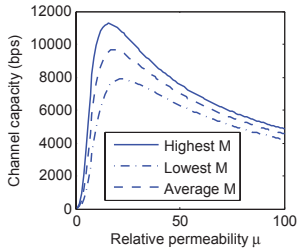

Fig. 13. Optimal μ for different mutual inductions.

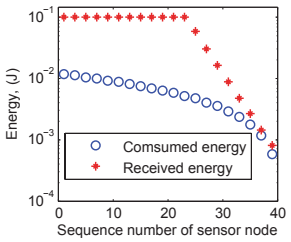

Fig. 14. Received energy & consumed energy.

According to [26], the channel capacity can be calculated by:

$$C_{MI} = \int_{f_L}^{f_U} log_2\left(1 + \frac{2P_t\pi^2 f^2 M^2}{R_c(R_c + \frac{4\pi^2 f^2 M^2}{R_c})N_{noise}}\right) \cdot df \ . \quad (25)$$

where P_t is the transmission power and N_{noise} is the noise power. Since the coils are loosely coupled to each other, $4\pi^2 f^2 M^2$ is much smaller than R_c. Hence, $\frac{4\pi^2 f^2 M^2}{R_c}$ is very small and can be neglected. Then, the closed form of (25) can be approximately obtained:

$$C_{MI} \simeq f_U \log_2\left(1 + \frac{2\pi^2 P_t M^2 f_U^2}{R_c^2 N_{noise}}\right) - f_L \log_2\left(1 + \frac{2\pi^2 P_t M^2 f_L^2}{R_c^2 N_{noise}}\right) . \quad (26)$$

2) Optimal μ_1 to maximize uplink channel capacity: As discussed previously, the effective permeability inside the fracture, μ_1, can be adjusted by changing the additive in the high-μ proppants. In Section IV, we prove that higher μ_1 has no effect on the downlink channel but can significantly reduce the path loss in the uplink channel. In this subsection, we analyze the effect of μ_1 on the uplink channel capacity. On the one hand, (18) and (19) show that the high-μ environment can reduce path loss in the uplink channel. On the other hand, (24) shows that the high-μ environment can also reduce the bandwidth of the channel. Therefore, there exists an optimal value for μ in the fracture to maximize the uplink channel capacity. Here we utilize the numerical method to identify the optimal value.

We set the transmission power as -20 dBm. The measured underground noise level is around -100 dBm in [27]. Due to the high temperature and complicated components in the oil reservoir, we set the noise power as -80 dBm. Since there is no measured noise level in oil reservoir at this moment, we use a higher noise. The distance between the transmitter and receiver is 1 m. Other parameters are the same as previous sections. Due to the random orientation of the tri-directional coil, the mutual induction M is not a constant. We consider the largest, smallest and average mutual induction. The results are shown in Fig. 13. It indicates that the channel capacity reaches its maximum value when μ is around $20\mu_0$. It's worth noting that this result is a local optimized value that is subjected to the transmission power, noise power, coil size, number of turns ,and transmission distance. The global optimal value can be found by taking all the variables into account. However, it is out of our scope in this paper.

According to Fig. 13, with the optimal μ_1, the achievable data rate can be higher than 8 kbps. Then the transmit/receive time can be calculated based on the data length and the data rate, which completes the energy consumption model for oil reservoir sensor networks.

C. Self-Contained System Performance

So far, the energy transfer model and energy consumption model are derived. In this subsection, we utilize the two energy models to check whether the proposed oil reservoir sensor network is self-contained or not, i.e. whether the sensors deep inside oil reservoirs can utilize the energy transferred from the dipole to wirelessly transmit sensing data back to the base station. The system parameters are set as follows. As suggested in [28], P_{tx}=31.5 mW, P_{rx}=1.8 mW, and T_{st}=800 μs. Here we set P_{out}=-20 dBm. According to (23) and (25), the bandwidth and channel capacity of the proposed system are higher than 1.6 kHz and 8 Kbps, even in the worst case. We set the length of the packet is 8 Bytes. Then $T_{on-tx/rx}$=8 ms. Thus, the transmitting energy is E_t=0.273 mJ and the receiving energy is E_r=15.8 μJ. The capacity E_{max} of the ultra capacitor is 0.1 J and the energy conversion rate η is 90%. There are 40 sensor nodes deployed in the fracture and the interval between two neighbors is 1 m. Noted that, for the downlink channel, we use tri-directional coil antenna as receiver. The path loss here we use is the maximum value which is almost the minimum value for the uni-directional coil antenna as shown in Fig. 11. We assume the charging time T_c is six hours. During each cycle, all the sensor nodes are first charged and then report their measurements back.

Fig. 14 shows the received energy in six hours and the consumed energy by each sensor node. The sequence number of the sensor node also indicates the distance between the sensor node and the dipole antenna in meters. The result shows that even the last sensor node that is farthest from the base station can receive enough energy for scheduled operation. It should be noted that although the last sensor node receives the minimum energy, it only sends out one packet from itself and does not relay packets. Meanwhile, although the first sensor nodes need to relay the data from all the other sensors, it also receives the maximum amount of energy that is more than enough. Interestingly, the bottleneck of the proposed system is neither the last nor the first sensor node, but the sensors numbered 36, 37, and 38 in Fig. 14. These nodes receive similar energy as the last node, but they need to relay the packets from the sensor nodes behind them. Therefore, the duty cycle should be long enough to allow enough charging time so that those "bottleneck" nodes can receive enough energy to work. We find that if the last sensor is closer to the base station, the charing time can be significantly reduced. For example, if we deploy the last sensor at the distance 35 m, the duty cycle can be reduced to 1.5 hours.

V. Conclusion

The real-time and in-situ oil reservoir monitoring system requires a self-contained and micro-sized wireless sensor network. However, due to the micro device size and the harsh oil reservoir environments, existing wireless communication and networking solutions do not work. In this paper, we propose a MI-based wireless sensor network framework for oil reservoir monitoring applications. We develop analytical channel and energy models to characterize the downlink from the wellbore base station to the millimeter-scale sensors deep inside oil reservoirs and the multi-hop uplink from the sensors

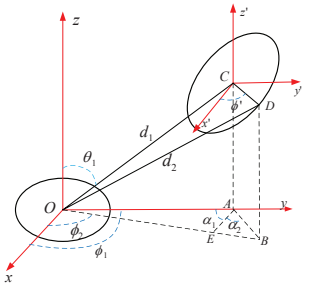

Fig. 15. Spherical coordination of point D.

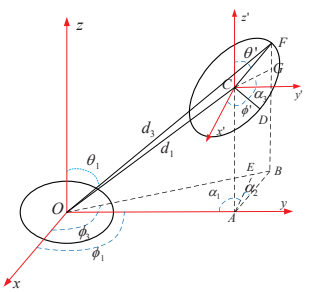

Fig. 16. Spherical coordination of point F.

back to the base station. Moreover, we propose to utilize the high-μ proppants and the tri-directional coil antenna that can significantly enhance the system efficiency and reliability. The theoretical models are validated by the Comsol Multiphysics-based simulations. Based on the analytical models and simulation results, we prove that: 1) the dipole can effectively transfer energy to the micro sensor nodes that are at least 40 m inside the fractures in oil reservoirs; 2) by utilizing the received energy, the micro sensor nodes can use MI communication mechanism transmit the sensing results back to the base station through a multi-hop fashion. Hence, this paper proves the feasibility of using wireless sensor networks to achieve the in-situ and real-time monitoring deep inside oil reservoirs.

In the future, the proposed framework can be further improved: 1) *coverage extension:* although this paper proves the proposed sensor system can be self-contained if the deepest sensor is within 40 m inside the oil reservoir, there is still significant room to extend the coverage distance if the key system parameters can be optimally determined, including the global optimal effective permeability inside the fracture, the system operating frequency for energy transfer and communication, among others; and 2) *energy efficient networking:* since the sensor nodes are densely deployed while their sensing results are highly correlated, optimal sampling schedule throughout the whole network can be designed to enable the sensor system provide more accurate measurements, consume less energy, and cover deeper sections inside the oil reservoir fractures.

Acknowledgment

The authors would like to thank Prof. Edward P. Furlani for his great support in the Comsol-based simulations.

Appendix

Modeling the Arbitrary Orientation of MI Coil

When deploying the wireless sensor nodes in oil reservoirs, it is impossible to control the orientation of the coil antenna on each sensor. Hence, the analysis on the effects of the coil orientation is of great importance. In Section IV, more specifically, (9), (12), and (18), the effects of the coil orientation are captured by the dot product of a unit normal vector of the targeted coil, i.e. "$\cdot\mathbf{n}$". In this appendix, we present the strategy on how to derive this normal vector of a unidirectional coil with arbitrary orientation.

We assume the spherical coordination of the coil's center is C $(d_1,\ \theta_1,\ \phi_1)$. The orientation of the coil is (θ', ϕ'), which are defined in Fig. 3. To derive the normal vector $\mathbf{n}$, we need to find the spherical coordinations of two non-overlapping points on the coil, since these two points together with the coil center can determine coil's the orientation. We denote these two points as D and F, as shown in Fig. 15 and Fig. 16. CD is the intersection of the coil and the $x'y'$ plane, while CF is perpendicular to CD. It should be noted that the coil and $x'y'$ plane have two intersections, we only consider the one on the right hand side.

A. Spherical Coordination of D

In Fig. 15, $\angle AOB$ is used to calculate the length of OB. AE is parallel with the axis x and x'. It's obvious that $\alpha = \alpha_1 + \alpha_2$. Since $\phi_1 = \pi/2$,

$$\alpha = \begin{cases} \frac{\pi}{2} + \phi',\ when\ \phi' \in [0,\ \frac{\pi}{2}] \cup (\pi,\ \frac{3\pi}{2}] \\ -\frac{\pi}{2} + \phi',\ when\ \phi' \in (\frac{\pi}{2},\ \pi] \cup (\frac{3\pi}{2},\ \pi]. \end{cases} \tag{27}$$

By utilizing the law of cosines, we obtain:

$$d_2 = \sqrt{d_1^2 + r^2 - 2d_1 r \sin\theta_1 \cos\alpha}\,. \tag{28}$$

Once we have d_2, θ_2 can be calculated by $\cos\theta_2 = d_1\cos\theta_1/d_2$, which is:

$$\theta_2 = \cos^{-1}\frac{d_1\cos\theta_1}{\sqrt{d_1^2 + r^2 - 2d_1 r\sin\theta_1\cos\alpha}}\,. \tag{29}$$

Finally, ϕ_2 can be obtained by using ϕ_1 and $\angle AOB$. Hence,

$$\phi_2 = \begin{cases} \frac{\pi}{2} - \beta,\ when\ \phi' \in [0,\ \frac{\pi}{2}] \cup (\pi,\ \frac{3\pi}{2}] \\ \frac{\pi}{2} + \beta,\ when\ \phi' \in (\frac{\pi}{2},\ \pi] \cup (\frac{3\pi}{2},\ \pi] \end{cases}, \tag{30}$$

where $\beta = \cos^{-1}(\frac{d_1\sin\theta_1 - r\cos\alpha}{\sqrt{d_1^2\sin^2\theta_1 + r^2 - 2d_1 r\sin\theta_1\cos\alpha}})$.

B. Spherical Coordination of F

As shown in Fig. 16, we choose the point F that is $\pi/2$ ahead of D. Then $\alpha = \alpha_1 + \alpha_2$, or

$$\alpha = |\pi - \phi'|\,. \tag{31}$$

Similarly as in calculating point D, we can find $d_3,\ \theta_3,\ and\ \phi_3$, which are:

$$d_3 = \sqrt{r^2 + d_1^2 + 2rd_1\cos\theta_1\cos\theta' - 2d_1 r\sin\theta_1\sin\theta'\cos\alpha}\,; \tag{32}$$

$$\theta_3 = \cos^{-1}\frac{d_1\cos\theta_1 + r\cos\theta'}{\sqrt{r^2 + d_1^2 + 2rd_1\cos\theta_1\cos\theta' - 2d_1 r\sin\theta_1\sin\theta'\cos\alpha}}\,. \tag{33}$$

Since we only consider the right point of the intersections between the coil and $x'y'$ plane, so point B is always on the left side of x' axis. So

$$\phi_3 = \frac{\pi}{2} + \beta\,, \tag{34}$$

where $\beta = \cos^{-1}(\frac{d_1\sin\theta_1 - r\sin\theta'\cos\alpha}{\sqrt{r^2\sin^2\theta' + d_1^2\sin^2\theta_1 - 2d_1 r\sin\theta_1\sin\theta'\cos\alpha}})$.

C. Deriving the Normal Vector of a MI Coil with Arbitrary Orientation

With the coordinations of three points on the plane of the coil, i.e. C $(d_1,\ \theta_1,\ \phi_1)$, D $(d_2,\ \theta_2,\ \phi_2)$, F $(d_3,\ \theta_3,\ \phi_3)$, the cartesian coordinations of the three points can be retrieved from those spherical coordinations. After acquiring the cartesian coordinations, we can construct three vectors on the plane of the coil and the normal vector $\mathbf{n}$ is perpendicular to all of them. Then, the normal vector $\mathbf{n}$ of the coil that goes through the center C can be analytically derived.

References

[1] Z. Sun and B. Zhu, "Channel and energy analysis on magnetic induction-based wireless sensor networks in oil reservoirs," in *Proc. 2013 IEEE ICC*.

[2] D. Chapman and W. Trybula, "Meeting the challenges of oilfield exploration using intelligent micro and nano-scale sensors," in *Proc. 2012 IEEE International Conference on Nanotechnology*.

[3] M. A. Braik, H. Nasr, and F. Saghir, "New wireless sensor network monitors water-injection wells off Abu Dhabi," *Oil & Gas Journal*, vol. 106, no. 44, Nov. 2008.

[4] W. C. Lyons and G. J. Plisga, *Standard handbook of Petroleum and Natural Gas Engineering*. Burlington, MA; Oxford, UK: Gulf Professional Pub., 2005.

[5] G. J. Elbring, L. W. Lake, M. F. Wheeler, R. Banchs, and S. P. Cooper, "Analysis of real-time reservoir monitoring: reservoirs, strategies and modeling," Sandia National Laboratories, Tech. Rep., 2006.

[6] D. L. Gysling and F. X. T. Bostick, "Changing paradigms in oil and gas reservoir monitoring - the introduction and commercialization of in-well optical sensing systems," in *Proc. 2002 Optical Fiber Sensors Conference Technical Digest*, vol. 1, pp. 43–46.

[7] A. Tamburini, M. Bianchi, C. Giannico, and F. Novali, "Retrieving surface deformation by psinsartm technology: a powerful tool in reservoir monitoring," *International Journal of Greenhouse Gas Control*, no. 4, pp. 928–937, 2010.

[8] O. Duru and R. N. Horne, "Modeling reservoir temperature transients, and matching to permanent downhole gauge (pdg) data for reservoir parameter estimation," in *Proc. 2008 SPE Annual Technical Conference and Exhibition*.

[9] I. F. Akyildiz and M. C. Vuran, *Wireless Sensor Networks*. Hoboken, NJ: John Wiley & Sons Inc, Aug. 2010.

[10] Micro sensor motes successfully travel through a canadian heavy oil reservoir. [Online]. Available: http://www.incas3.eu/news

[11] M. A. Akkas, I. F. Akyildiz, and R. Sokullu, "Terahertz channel modeling of underground sensor networks in oil reservoirs," in *Proc. 2012 IEEE GLOBECOM*.

[12] Z. Sun and I. F. Akyildiz, "Magnetic induction communications for wireless underground sensor networks," *IEEE Trans. Antennas Propag.*, vol. 58, no. 7, pp. 2426–2435, July 2010.

[13] A. K. RamRakhyani, S. Mirabbasi, and M. Chiao, "Design and optimization of resonance-based efficient wireless power delivery systems for biomedical implants," *IEEE Trans. Biomed. Circuits Syst.*, vol. 5, no. 1, pp. 48–63, Feb. 2011.

[14] W. M. Merrill, R. E. Diaz, M. M. Lore, M. C. Squires, and N. G. Alexopoulos, "Design and optimization of resonance-based efficient wireless power delivery systems for biomedical implants," *IEEE Trans. Antennas Propag.*, vol. 47, no. 1, pp. 142–148, Jan. 1999.

[15] D. R. Frankl, *Antenna Theory*. Englewood Cliffs, 2005.

[16] C. A. Balanis, *Antenna Theory: Analysis and Design*, 2nd ed. Hoboken, NJ: John Wiley & Sons Inc., 2005.

[17] P. Diament, *Wave Transmission and Fiber Optics*. New York, NY: Macmilan Publishing Company, 1990.

[18] Z. Jia, G. Yan, H. Liu, Z. Wang, P. Jiang, and Y. Shi, "The optimization of wireless power transmission: design and realization," *The International Journal of Medical Robotics and Computer Assisted Surgery*, vol. 8, no. 3, pp. 337–347, Sept. 2012.

[19] A. Markham and N. Trigoni, "Magneto-inductive networked rescue system (miners) taking sensor networks underground," in *Proc. 2012 IPSN*.

[20] R. Carta, M. Sfakiotakis, N. Pateromichelakis, J. Thone, D. P. Tsakiris, and R. Puers, "A multi-coil inductive powering system for an endoscopic capsule with vibratory actuation," *Sensors and Actuators A: Physical*, vol. 172, no. 1, pp. 253–258, 2011.

[21] R. Puers, R. Carta, and J. Thone, "Bordersense: border patrol through advanced wireless sensor networks," *Journal of Micromechanics and Microengineering*, vol. 21, no. 5, 2011.

[22] P. Jourand, R. Carta, and R. Puers, "Dedicated clss-e driver for large area wireless medical inspection capsules," *Procedia Engineering*, vol. 25, pp. 1004–1007, 2011.

[23] E. Shih, S. H. Cho, N. Ickes, R. Min, A. Sinha, A. Wang, and A. Chandrakasan, "Physical layer driven protocol and algorithm design for energy-efficient wireless sensor networks," in *Proc. 2001 International Conference on Mobile Computing and Networking*, pp. 272–287.

[24] P. Grover and A. Sahai, "Shannon meets tesla: wireless information and power transfer," in *Proc. 2010 IEEE ISIT*.

[25] Z. Sun and I. F. Akyildiz, "On capacity of magnetic induction-based wireless underground sensor networks," in *Proc. 2012 IEEE INFOCOM*.

[26] Z. Sun, I. F. Akyildiz, S. Kisseleff, and W. Gerstacker, "Increasing the capacity of magnetic induction communications in rf-challenged environments," *IEEE Trans. Commun.*, vol. 61, no. 9, pp. 3943–3952, Sept. 2013.

[27] L. Li, M. C. Vuran, and I. F. Akyildiz, "Characteristics of underground channel for wireless underground sensor networks," in *Proc. 2007 Med-Hoc-Net*.

[28] C. C. Enz, A. El-Hoiydi, J. Decotignie, and V. Peiris, "Wisenet: an ultralow-power wireless sensor network solution," *Computer*, vol. 37, no. 8, pp. 62–70, 2004.

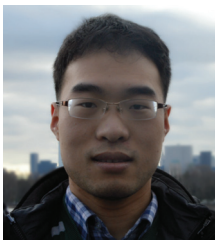

Hongzhi Guo (S'12) received the B.S. degree in Automation from Shandong University of Science and Technology, Qingdao, China, and the M.S. degree in Electrical Engineering from Columbia University, New York, NY, in 2011 and 2013, respectively. Currently, he is a Ph.D. student in the Electrical Engineering Department at State University of New York at Buffalo, Buffalo, NY. His current research interests are in wireless communications, and wireless sensor networks.

Zhi Sun (M'11) received the B.S. degree in Telecommunication Engineering from Beijing University of Posts and Telecommunications (BUPT), and the M.S. degree in Electronic Engineering from Tsinghua University, Beijing, China, in 2004 and 2007, respectively. He received the Ph.D. degree in Electrical and Computer Engineering from Georgia Institute of Technology, Atlanta, GA. in 2011. Currently, he is Assistant Professor in the Electrical Engineering Department at State University of New York at Buffalo, Buffalo, NY. Prior to that, he was a Postdoctoral Fellow at Georgia Institute of Technology, Atlanta, GA. Dr. Sun has won the Best Paper Award in the 2010 IEEE Global Communications Conference (Globecom). He received the BWN researcher of the year award at Georgia Institute of Technology in 2009. He was also given the outstanding graduate award at Tsinghua University in 2007. His expertise and research interests lie in wireless communications, wireless sensor networks, and cyber physical systems in challenged environments. He is a member of the IEEE.